Advanced Steel Construction – Vol. 20 No. 2 (2024) 125–134
DOI:10.18057/IJASC.2024.20.2.4
(Special Issue: *11st International Conference on Advances in Steel Structures, ICASS'2023, Kuching, Sarawak, Malaysia*)

BEHAVIOR INSIGHTS AND PLASTIC DESIGN CONSIDERATIONS OF SSTF SYSTEMS BASED ON DETAILED FINITE ELEMENT ANALYSES OF A PROPOSED SUB-STRUCTURE

Ze-Xiang Li [1], Dan Gan [1,*], Xu-Hong Zhou [2] and Xi Lu [2]

[1] *School of Civil Engineering and Geomatics, Southwest Petroleum University, Chengdu 610500, China*
[2] *School of Civil Engineering, Chongqing University, Chongqing 400045, China*
** (Corresponding author: E-mail: gandan@cqu.edu.cn)*

ABSTRACT

The steel staggered truss framing (SSTF) system has been increasingly utilized due to its large column-free spaces, high construction efficiency, and favorable economic benefits. Despite its advantages, the SSTF system has yet to be incorporated in mainstream seismic design codes and is predominantly applied in low-seismic regions. The primary obstacle hindering the wider application of the SSTF system is the limited understanding of its inelastic behaviors, particularly in regard to diaphragm actions. This study firstly introduces an SSTF sub-structure that precisely reflects the diaphragm actions and the structural behaviors of SSTF systems, facilitating experimental researches and finite element (FE) analyses. Subsequently, a detailed SSTF sub-structure FE model and a pure steel truss FE model, considering the diaphragm actions and gusset plate connections, were established based on a plastically designed prototype SSTF structure in previous study. The yielding mechanism of the chord members, inelastic behaviors of the diaphragms, lateral responses, and stress distributions of the web members were investigated. Lastly, plastic design considerations involving the classification of the rigidity of the diaphragm, rotation demand of the chord member, mechanical calculation model of the truss and amplification factor of the web members were given to facilitate achieving the expected ductile failure mode of SSTF systems.

ARTICLE HISTORY

Received: 8 April 2024
Revised: 30 April 2024
Accepted: 5 June 2024

KEYWORDS

Steel staggered truss framing system;
Diaphragm action;
Inelastic behavior;
Sub-structure;
Finite element analysis

1. Introduction

A steel staggered truss framing (SSTF) system (see Fig. 1) is mainly composed of a series of transverse story-high trusses, columns, longitudinal framing beams, and diaphragms [1]. The large-span trusses are staggered arranged at the adjacent column lines, which creates large column-free spaces for flexible layouts. In the middle of the trusses, a Vierendeel panel without diagonal web member is usually adopted to build a practical corridor and increase the ductility of the trusses [2]. The truss members and columns in a SSTF system are mainly subjected to axial forces, which are efficient in carrying loads and reducing steel consumption [3]. The columns are arranged on the perimeter of the structure only, which reduces superstructure weight and saves foundation cost. In general, SSTF systems have the advantages of large lateral stiffness, large column-free space, reduced steel consumption, low foundation cost, and quick erection, and this system is suitable for multi-story residential buildings, dormitories, hotels, and office buildings [4,5].

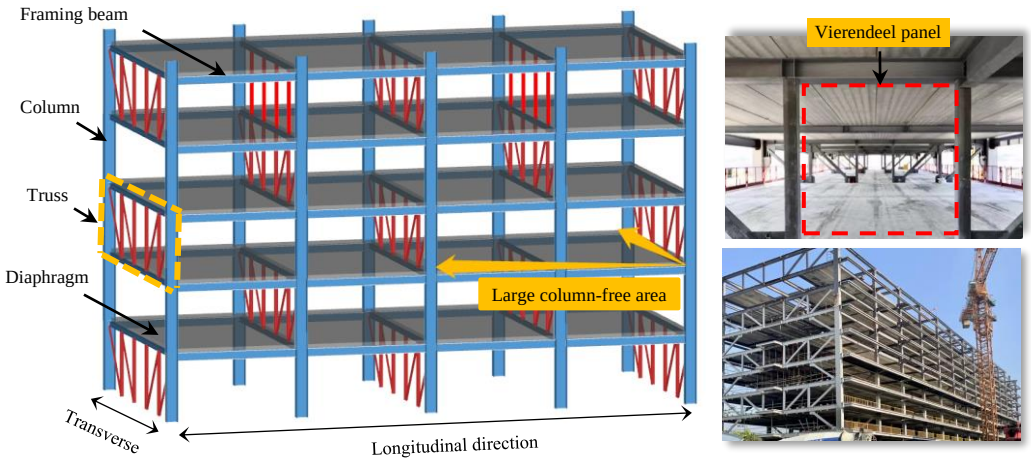

Fig. 1 SSTF systems

Since the SSTF system originated in 1960s [1], continuous researches on the load-carrying behaviors, design solutions and seismic performances were conducted. Gupta and Goel [3] conducted inelastic dynamic analyses of a SSTF system with a proposed computational analytical model. High seismic performance of the system was proved: only the chord members in the Vierendeel panels yielded when the structure was subjected to 1.5 times the ground motion of the 1940 EI Centro earthquake. Hanson and Robert [6] presented an elastic limit-ultimate strength design procedure for earthquake resistant response of multi-story SSTF buildings concentrating the inelastic activity at the chord members in the Vierendeel panels. Kim et al. [7] conducted nonlinear static analyses of SSTF buildings to identify their failure modes under seismic loads. The Design Guide 14: Staggered Truss System Framing Systems [8], published by AISC, provides an all-round process for the primary design of a SSTF system. Simasathien et al. [9] adopted additional diagonal members, multiple Vierendeel panels and horizontal trusses to enhance the seismic performance of SSTF systems. Kim et al. [10,11] introduced kinds of strategies including interior columns, vertical cables, end braces, and buckling-restrained braces to improve the seismic performance of SSTF systems and developed a performance-based seismic design method for SSTF structures equipped with friction dampers in the Vierendeel panels. Zhou et al. [12] quantified the inelastic seismic demand of a novel SSTF system showing damage-control behavior by using a probabilistic seismic demand spectral surface model.

The above studies paid extensive interest on the seismic performance of SSTF systems but, for various reasons, did not account for the influence of diaphragm actions. It should be noted that the diaphragm constitutes a vital component of the lateral load-resisting system of SSTF systems. Due to the staggered arrangement of the trusses, the diaphragms need to transmit the top-down lateral loads from the trusses. The diaphragm actions, including the out-of-plane stiffness, the inelastic behavior, and the interactions to the trusses, affect the lateral stiffness, load distribution, and failure mechanism of SSTF systems [13]. Up to now, the SSTF system is not included in the mainstream seismic design codes. The practical engineering projects of SSTF systems are mainly located in low-seismic regions. Some works still need to be done to figure out the inelastic behavior and failure mechanism of SSTF systems.

The seismology committee of the Structural Engineers Association of California (SEAOC) holds that the SSTF system is not a basic seismic-force-resisting system and more tests and analyses considering the diaphragm actions should be performed, as opposed to just the behavior of individual components [14]. Several experimental studies of SSTF systems were conducted [15–18]. However, either bare steel plate diaphragms were used or the sources of the diaphragm behavior were not given, and the tested SSTF systems exhibited relatively poor ductility due to the premature failure of the web members or column base. In addition, experimental researches or refined finite element (FE) analyses of an entire structural system induce significant costs.

To facilitate conducting in-depth experimental studies and FE analyses of SSTF systems, an SSTF sub-structure which accurately reflect the diaphragm actions and the structural behaviors of SSTF systems was proposed in this work. Subsequently, detailed FE models considering the inelastic behavior of diaphragms and the effects of the gusset plate connections were established and the behavior insights of the SSTF system were studied. Lastly, several plastic design considerations for SSTF systems to achieve the expected ductile failure mode were given.

2. Verification of the SSTF sub-structure

In an SSTF system, the diaphragms and the trusses constitute the lateral load-resisting systems in the transverse direction. Fig. 2 illustrates the smallest lateral load-transmitting element of an SSTF system. The seismic loads or the wind loads from the upper truss are transmitted by the diaphragm to the lower two trusses, and thereby to the foundation step by step. However, the boundary conditions of chord members are difficult to precisely set up due to the vertical and lateral deformation of the chord members when this element is subjected to lateral loads. In addition, the trusses are prone to suffer out-of-plane instability.

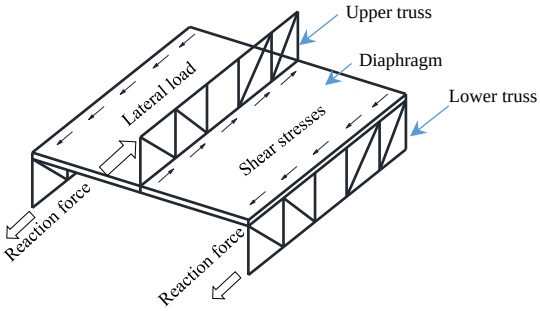

Fig. 2 The lateral load-resisting element of SSTF systems

Therefore, an SSTF sub-structure comprising a typical truss, two diaphragms, six columns, eight beams, and four side chord members is proposed herein, extracted from a prototype SSTF structure, as shown in Fig. 3. Hinged supports are set at the four exterior column bases since there is almost no bending moment at the columns while SSTF structure subjected to transverse lateral loads. Transverse sliding supports whose vertical and longitudinal degrees of freedom are constrained are set at the two interior column bases. This provides the truss with supports while allows in-plane deformation of the lower diaphragm. Lateral loads are applied at the top ends of the four exterior columns. In the sub-structure, the applied lateral loads are transmitted to the truss through the top diaphragm, and finally to the hinged supports through the bottom diaphragm. The features of the SSTF system that diaphragms transmit the shear forces between the staggered trusses and the interaction of the diaphragm and truss are thereby reflected by the sub-structure. Most importantly, the sub-structure facilitate experimental researches or FE analyses due to its simple boundary conditions. In addition, it is a stable three-dimensional spatial structure that does not require additional supports when conducting experimental research.

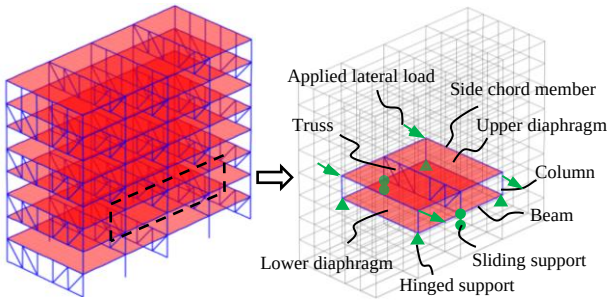

Fig. 3 A typical SSTF sub-structure

In previous study, an analysis model of an plastically designed example SSTF structure with diaphragm based on nonlinear multi-layered shell elements was established and transverse pushover analysis was conducted [13]. Based on the previous study, pushover analysis of the sub-structure extracted from the prototype SSTF structure was conducted. And then, the shear force versus lateral displacement relationships of the same truss from the prototype SSTF structure and the sub-structure were collected and compared. The horizontal force components of the chord members and the vertical web members were neglected, as shown in Fig. 4.

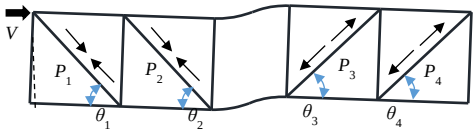

Fig. 4 Shear force of the truss

Therefore, the shear force of the truss can be calculated by accumulating the horizontal force components of the diagonal web members:

$$V = P_1\cos\theta_1 + P_2\cos\theta_2 + P_3\cos\theta_3 + P_4\cos\theta_4 \quad (1)$$

As shown in Fig. 5, the shear force versus lateral displacement relations of the trusses from the sub-structure and the prototype SSTF structure kept almost the same. Therefore, the proposed sub-structure precisely predicts lateral responses of the SSTF structure and can be used to conduct further FE analyses to explore the inelastic behavior of SSTF systems considering diaphragm actions.

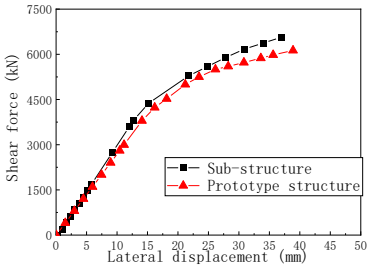

Fig. 5 The shear force versus lateral displacement curves of the trusses

3. Finite element model

3.1. Model description

A detailed FE model of an SSTF sub-structure established by the software ABAQUS [19] is shown in Fig. 6. The boundary conditions were set as mentioned above. Four-node reduced integral shell (S4R) elements were employed to model the steel members including the truss, the columns, the beams, the side chord members and the gusset plates. Eight-node incompatible solid (C3D8I) elements were employed to model the concrete floor slabs, as C3D8I elements were found to be more efficient in modelling plate components without mesh distortions, and could reduce the number of grid units and shorten

the calculation time [20]. Two-node three-dimensional truss (T3D2) elements were employed to model the reinforcements. The chord member in the Virendeel panel and the adjacent diaphragm will inevitably produce significant plasticity. To accurately capture the interaction behavior of the diaphragm and chord member at the Vierendeel panel, seven studs based on four-node shell element (S4) were set at the Vierendeel panel (plastic hinge zone), as recommended by Yin and Shi [21]. Six nodes of each stud tied with the concrete slab. Hard contact was used in the normal direction of the interfaces between the chord and the concrete in the Vierendeel panel and the tangential friction coefficient of the interfaces was taken as 0.25. In the areas outside the Vierendeel panel, the floor slabs were tied in the top flanges of beams and the chord members. The element size was taken as 15 mm for the steel members and reinforcements and 100 mm for the floor slabs after sensitivity analysis. The floor slabs were discretized into four layers of mesh through thickness. All the steel members were merged as one part. The reinforcements were embedded in the concrete floor slabs.

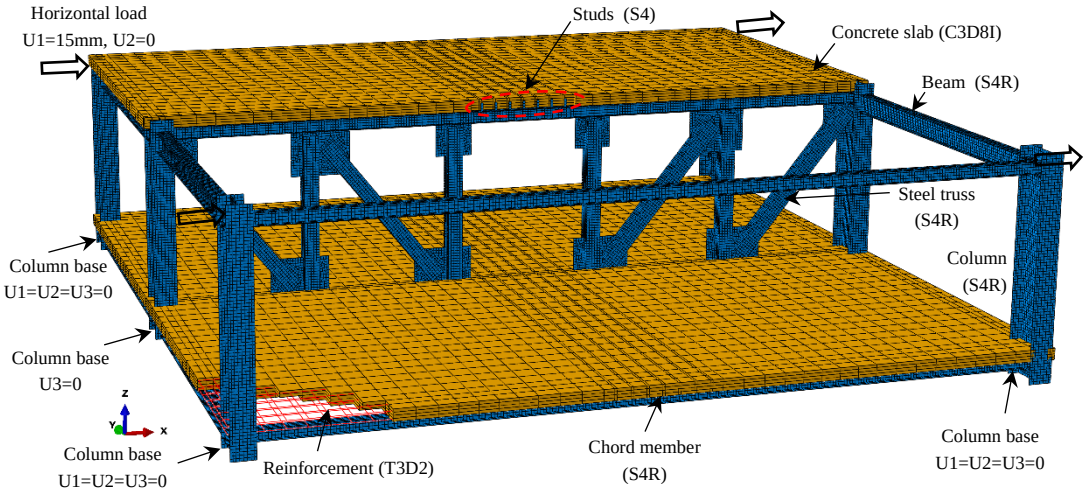

Fig. 6 FE model of the SSTF sub-structure

The prototype structure in Ref. [13] is plastically designed and realized the expected failure mode. The sub-structure model is 1/3 scaled of the prototype structure in Ref. [13], with the height of 1 m and the plane dimension of 4 m × 4 m. The detailed elevation arrangement of the truss is shown in Fig. 7. The dimensions of the steel members are listed in Table 1. The letter "H" denotes an H-section, with the subsequent four numbers signifying the section height, flange width, web thickness, and flange thickness, respectively. The letter "F" denotes a square-section, with the subsequent four numbers signifying the tube width and tube thickness, respectively. The thickness of the floor slabs was 60mm. The reinforcements were double layered and bi-directional in configuration. The diameter and spacing of the reinforcements were 8 mm and 100 mm, respectively.

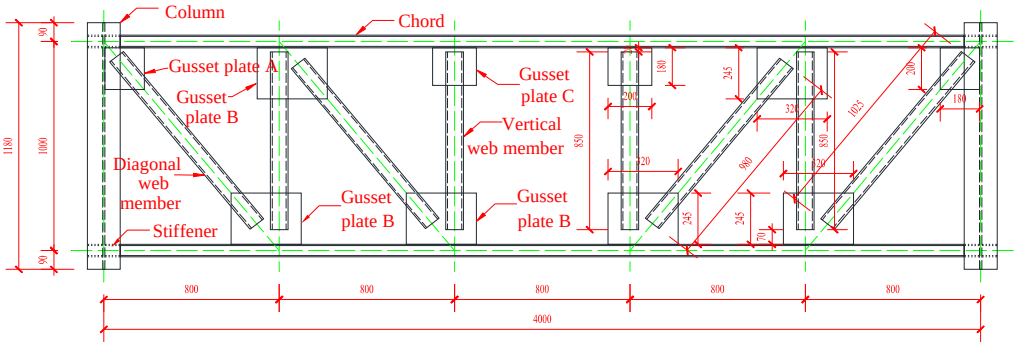

Fig. 7 Elevation of the truss (unit in mm)

Table 1
Dimensions of the steel members

Member	Sectional dimension (mm)
Column	H200×150×10×10
Beam	H100×80×6×6
Chord member	H60×60×6×6
Diagonal web member	F80×6
Vertical web member	F80×6
Gusset plate A	180×200×8
Gusset plate B	320×245×8
Gusset plate C	200×180×8

The elastic-perfectly plastic model was used for the steel members and reinforcements. The modulus of elasticity (E_s) and the Poisson's ratio of the steel members and reinforcements was taken as 200 GPa and 0.3, respectively. The steel grade of the Gusset plate was Q355 (yield strength f_y = 355 MPa) and the steel grade of the other steel members was Q235 (yield strength f_y = 235 MPa). The reinforcement grade was HRB400 (yield strength f_{yr} = 400 MPa).

The concrete grade of the floor slabs was C30 (compressive strength f_c = 24 MPa). Modulus of elasticity of concrete (E_c) was taken as $4700(f_c)^{0.5}$ [22]. The plastic damage model of concrete was adopted and the detailed parameters are shown in Table 2.

Table 2
Dimensions of the steel members

Dilation angle (ψ)	Flow potential eccentricity (e)	f_{bo}/f_c	Compressive meridian (K_c)	Viscosity parameter
31°	0.1	1.16	0.67	0.0001

where f_{bo}/f_c is the ratio of equal biaxial to uniaxial compressive strength of concrete.

The nonlinear uniaxial compressive behavior of the concrete from GB 50010 [23] was used. The stress-strain relationship was defined by Eqs. (2)–(6).

$$\sigma = (1-d_c)E_c\varepsilon \tag{2}$$

$$d_c = \begin{cases} 1-\dfrac{\rho_c n}{n-1+x^n} & (x \leqslant 1) \\ 1-\dfrac{\rho_c}{\alpha_c(x-1)^2+x} & (x>1) \end{cases} \tag{3}$$

$$\rho_c = \frac{f_c}{E_c\varepsilon_{cr}} \tag{4}$$

$$n = \frac{E_c\varepsilon_{cr}}{E_c\varepsilon_{cr} - f_c} \tag{5}$$

$$x = \frac{\varepsilon}{\varepsilon_{cr}} \tag{6}$$

where ε_{cr}=1640×10^{-6}, and α_c=1.36 when C30 concrete was used.

Fracture energy G_f was used to describe the tensile behavior of the concrete as suggested by mode specification Mode Code [24].

$$G_f = \alpha\left(0.1f_c\right)^{0.7} \tag{7}$$

where α is a parameter related to the sizes of concrete aggregate and taken as 0.03 in this investigation.

A damage variable d calculated by Eq. (8) [25] for concrete was used.

$$d = 1-\sqrt{\frac{\sigma}{E_c\varepsilon}} \tag{8}$$

A FE model of a pure steel truss was established for comparison, as shown in Fig. 8. The sizes, modelling methods and materials of the pure steel truss model were the same as the sub-structure model. Horizontal loads were applied at the top ends of the columns and hinged supports were set at the column bases. Lateral supports were set at the ends of the Vierendeel panel to prevent lateral torsion.

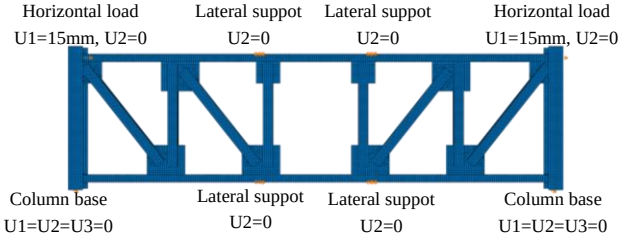

Fig. 8 FE model of the pure steel truss

3.2. Model validation

For conducting precise refined analysis of the sub-structure, the accurate prediction of the inelasicity of the Vierendeel panel of the truss and the interaction behavior between the RC concrete diaphragm and the chord member are of key importance. As mentioned above, the existing experimental results of SSTF systems are not suitable to be used to validate the FE model due to the lack of the sources of diaphragm behavior and inelasticity [15–18]. Also, there is no existing experiment of SSTF sub-structures. However, the developments of the special truss moment frames and eccentrically braced frames offer experimental sources to validate the FE model, since both of them allow a middle special segment to dissipate energy and improve the ductility of the structure, similar as SSTF structure [10,14]. Thus, available experimental results of a steel special truss moment frame with a Vierendeel panel under cyclic loads tested by Chao et al. [26] and an steel eccentrically braced frame with a floor slab under cyclic loads tested by Ciutina et al. [27] are used to validate FE model.

The elevation arrangement and test set up of the full scaled steel special truss moment frame specimen STMF1 are shown in Fig 9(a) and the counterpart FE model based on S4R elements is shown in Fig 9(b). The loading history, material properties, boundary conditions were the same as the test [26]. The double channel chord members and web members were tied with the gusset plates. Kinematic hardening rule was used in the validating.

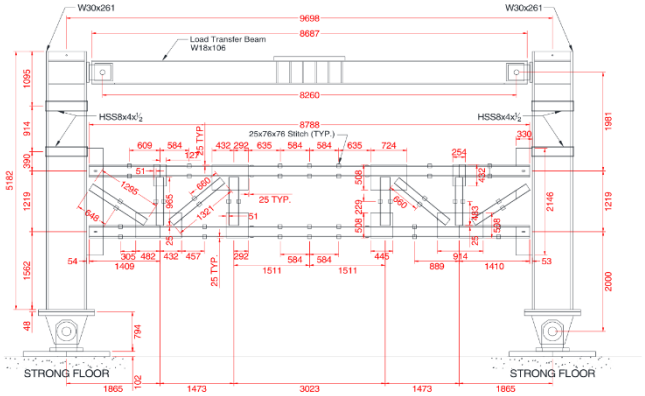

(a) Elevation arrangement and test set up (sourced from Ref. [26])

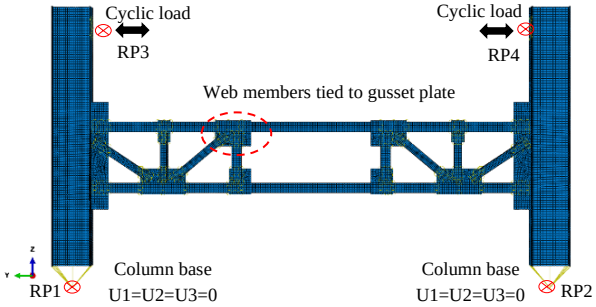

(b) FE model

Fig. 9 The special truss moment frame specimen STMF1

Only the chord member at the Vierendeel panel end yielded and the members outside kept elastic during the tests of specimen STMF1 [26]. Fig. 10(a) shows the yielding pattern of STMF1 at a story drift ratio (SDR) of 2%. It can be seen that the yielding pattern of the FE model shown in Fig. 10(b) is consistent well with the tested results.

Although considering fracture is conductive to the determination of the ultimate load-carrying capacity of the steel structural components [28,29], it is not essential to consider the cracking behavior of the chord member of the sub-structure since the current work focus on the inelastic behavior before its ultimate state. In the tests, the strength of STMF-1 started to degrade significantly at 3% SDR due to the fracture of the chord member [26]. As shown in Fig. 11, the lateral force versus displacement curve from FE analysis results coincides well with the tested results.

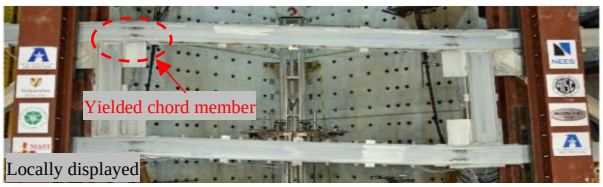

(a) Tested specimen STMF1 (sourced from Ref. [26])

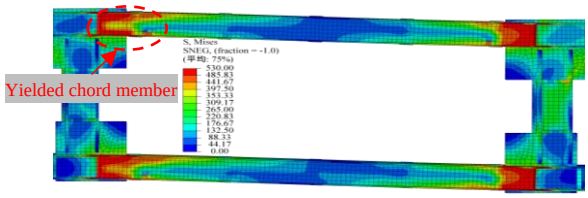

(b) FE analysis

Fig. 10 Comparison of the yielding pattern at 2% SDR

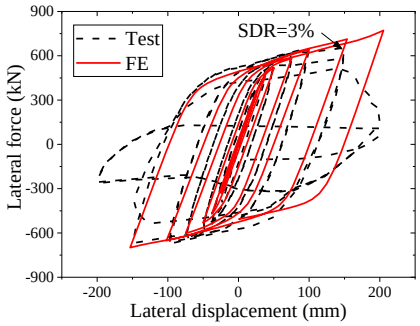

Fig. 11 Force versus displacement curves of test [26] and FE analysis

The elevation arrangement and test set up of the eccentrically braced frame specimen EBF-LF-Comp1 is shown in Fig. 12(a) and the counterpart FE model is shown in Fig. 12(b). The loading history, material properties, boundary conditions were the same as the test [27]. The modelling method of the steel members and the RC diaphragm was the same as the sub-structure descripted above. Kinematic hardening rule for the middle steel link beam was used.

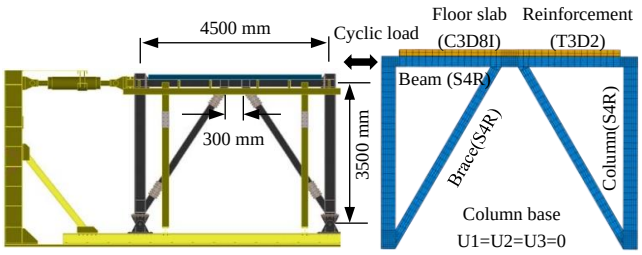

(a) Test set up (sourced from Ref. [27]) (b) FE model

Fig. 12 The eccentrically braced frame specimen EBF-LF-Comp1

The failure modes and lateral force versus displacement curves of the test specimen and the FE model are shown in Figs. 13 and 14, respectively. As seen, the FE model accurately predicts both the failure modes and the lateral responses of the tested composite eccentrically braced frame specimen before the specimen losing its load-carrying capacity due to the fracture of the link beam.

In general, the FE models acquired good predicting accuracy, including the yielding mechanism of the steel members, the inelasticity of the RC diaphragm, and the lateral behavior of the structures. Therefore, the modelling method is adequate to conduct further analysis of the SSTF sub-structure.

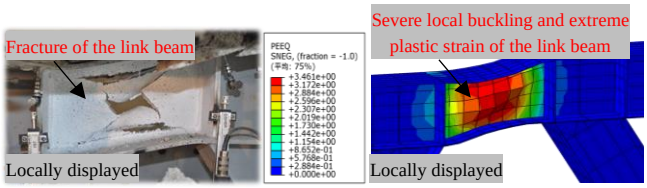

(a) steel link beam

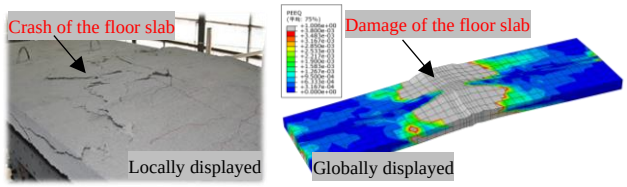

(b) floor slab

Fig. 13 Failure modes of the test [27] and FE analysis

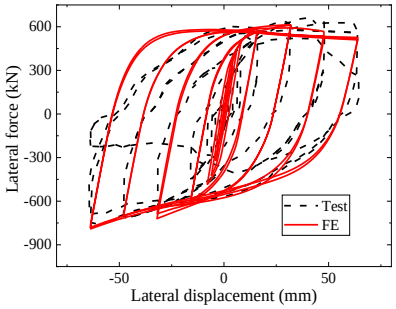

Fig. 14 Force versus displacement curves of the test [27] and FE analysis

4. Finite element analysis

4.1. Yielding patterns of the steel trusses

Fig. 15 shows the von Mises stress contour plot of the truss in the sub-structure model at the plastic SDR limit (stipulated as 1/75 by JGJ/T 329-2015 [30]). The expected yield mechanism was achieved. The chord member at the Vierendeel panel ends yielded sufficiently and the web members kept elastic.

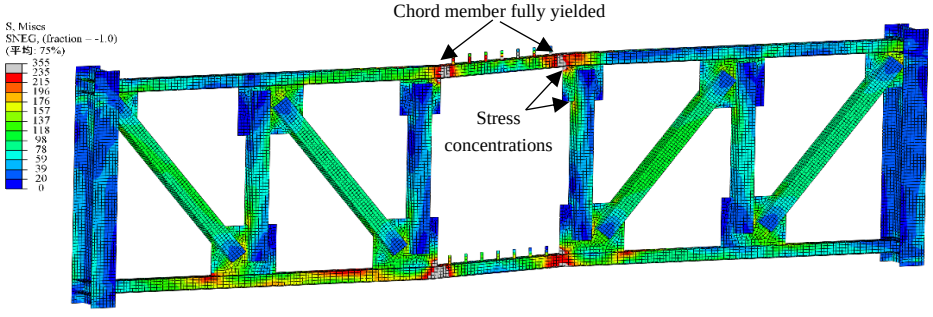

Fig. 15 Von Mises stress contour plot of the truss in the sub-structure model

However, it should be noted that there were stress concentrations near the Vierendeel panel, located at the vertical web member ends and the corners of the gusset plate C. The corners of the gusset plate C had yielded and the vertical web member ends nearly reached to the yield stress. The stresses were unevenly distributed at the vertical web members near the Vierendeel panel, which exhibited bending moment-subjecting characteristic. The stresses at the other web members were evenly distributed, which exhibited axial force-subjecting characteristic

Fig. 16 shows the von Mises stress contour plot of the pure steel truss model with the same SDR. The expected yield mechanism that the chord member at the Vierendeel panel ends yield firstly was achieved as well. It exhibited similar load-subjecting characteristics as the truss of the sub-structure. However, the stresses at the web members were much smaller than those of the sub-structure model, because the lateral stiffness of the pure truss model was much smaller than the sub-structure model (see the comparison of the skeleton curves below).

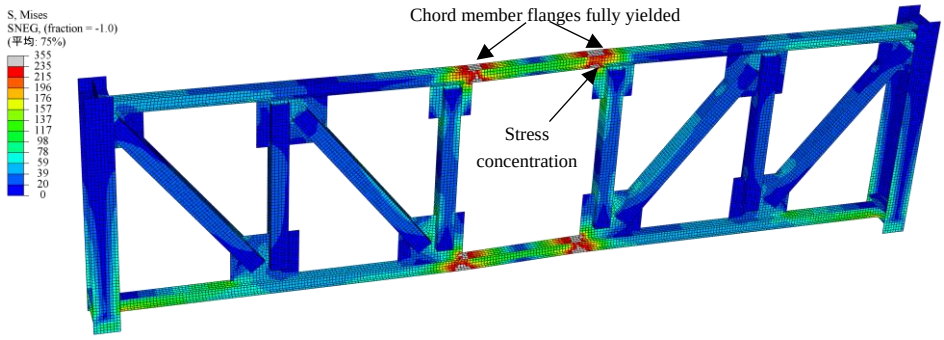

Fig. 16 Von Mises stress contour plot of the pure truss model

4.2. Behaviors of the RC diaphragms

Fig. 17 shows the equivalent plastic strain (PEEQ, defined by ABAQUS User's manual [19]) contour plots of the concrete slabs at 1/75 SDR. As seen, a damage area occurred at middle of the diaphragms while the areas else keep elastic. The stresses in the concrete slab is complicated since the diaphragms are subjected to combined in-plane and out-of-plane forces when the sub-structure is horizontal loaded, namely the shear forces transmitted to the truss and the passive moments caused by the rotation of the chord member in the Vierendeel panel. However, it is inferable that the damage at the diaphragms is a kind of ductile flexural failure caused by flexural stresses rather than brittle shear failure caused by shear stresses, which can be verified by the stress plot of the reinforcements and the hysteretic curve below. The diaphragms could still effectively transfer in-plane shear forces by the elastic concrete parts and the reinforcements at the plastic SDR limit, and thereby provides lateral stiffness of the SSTF structure for load-resisting.

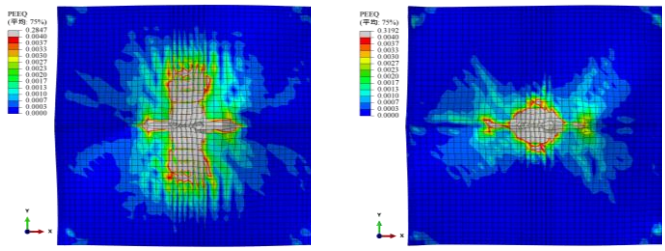

(a) Top concrete slab **(b)** Bottom concrete slab

Fig. 17 Damage of the concrete slabs

Fig. 18 shows the Von Mises stress contour plots of the reinforcements at 1/75 SDR. As seen, all the stress profiles consisted of two parts: the "X" type shear stresses penetrating the entire reinforcement mesh and the flexural stresses near the Vierendeel panel. The yielded reinforcements near the Vierendeel panel caused by passive moments coincided with the damage area of the concrete slab shown in Fig. 17.

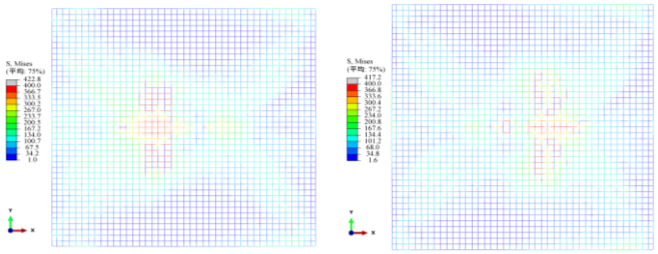

(a) Upper mesh of the upper diaphragm (b) Lower mesh of the upper diaphragm

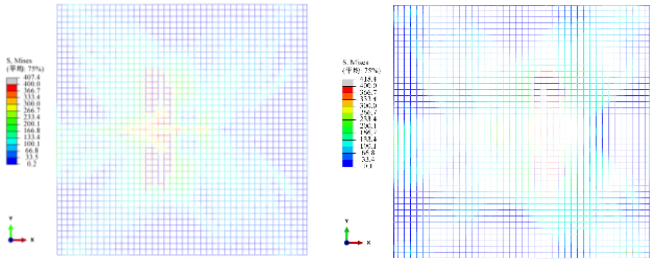

(c) Upper mesh of the lower diaphragm (d) Lower mesh of the lower diaphragm

Fig. 18 Damage of the concrete slabs

4.3. Lateral load versus displacement responses

Fig. 19 depicts the hysteretic curves of the sub-structure model and the pure truss model under lateral cyclic loads. The hysteretic curves were full due to the presence of expected failure mode, i.e., the chord members at the Vierendeel panel ends fully yielded and the web members kept elastic. After the chord member yielded, the hysteretic curve of the sub-structure model still slowly grew due to the increasing effective width of the RC diaphragms. This also supports the above argument about the failure modes of the concrete slab. Because once in-plane shear failure of the diaphragm occurred, the diaphragm would lose its function for load-transmitting and the sub-structure would lose its load-carrying capacity.

In the seismic design code GB50011-2010 [31], the elastic SDR limit for the steel structures is 1/250 and the plastic SDR limit is 1/50. In JGJ/T 329-2015 [30], the plastic SDR limit for SSTF structures in the transverse direction is tighten to 1/75 due to its relatively poor ductility while the elastic SDR is still stipulated as 1/250. As shown in Fig. 19, both the sub-structure model and the pure truss model yielded before the elastic SDR limit due to the relatively large rotation of the chord members [32,33]. In addition, the lateral stiffness of SSTF structures in the transverse direction is usually larger than the steel moment frames. Therefore, the existing elastic SDR limit of 1/250 for SSTF structures is too loose and might not fulfil the requirement of the "no damage in low-level earthquake". A stricter elastic SDR limit of 1/400 is recommended.

The diaphragms significantly enhanced the lateral stiffness and load-carrying capacity of the truss, as shown in the comparison of the skeleton curves of the two models (Fig. 20). The initial stiffness of the pure truss was 56 kN/mm, while that of the sub-structure model was 101 kN/mm (1.8 times the pure truss). The yield load was defined when the flange of the chord member yielded, i.e., the model entered inelastic stage. The yield load of the pure truss model was 149 kN, while that of the sub-structure model was 319 kN (2.1 times the pure truss). Therefore, the diaphragm actions in SSTF structures need to be considered, which is beneficial for correctly obtaining the internal force of the web members to realize the expected failure mode [13].

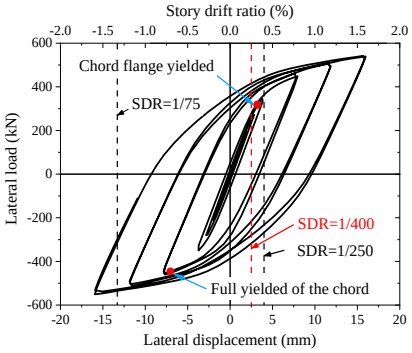

(a) Sub-structure

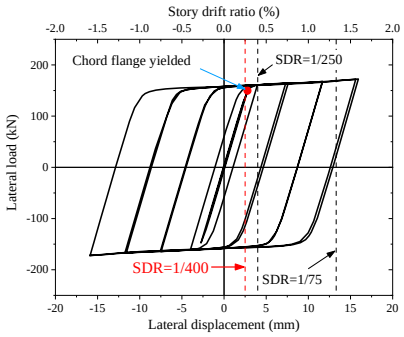

(b) Pure truss

Fig. 19 Hysteretic curves under lateral cyclic loads

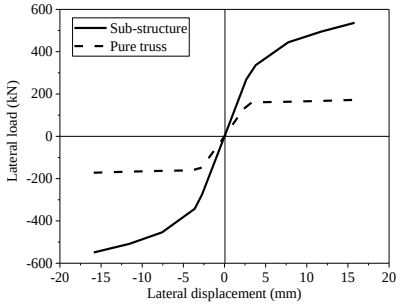

Fig. 20 Skeleton curves

4.4. Stress distributions at the web members

Longitudinal stresses at the vertical web member and the diagonal web member near the Vierendeel panel of the sub-structure model were extracted at 1/75 SDR. The positions of the extracted points are displayed in Fig. 21, located at the center and the corners of the top, middle and bottom sections of the web members.

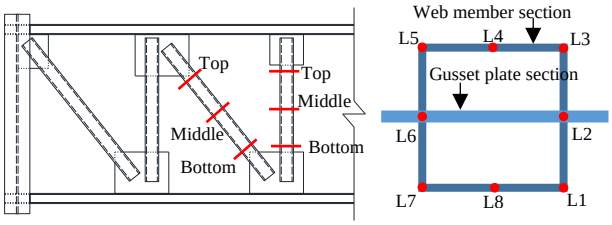

Fig. 21 The position of the extracted stresses

Fig. 22 shows the distribution of the longitudinal stresses at the vertical web member near the Vierendeel panel. Note that the positive values denote tensile stresses while the negative values denote compressive stresses. It could be seen that the stresses at the middle section were evenly distributed while the stresses at the top section and the bottom section were symmetrically distributed. Therefore, the vertical web member near the Vierendeel panel was subjected to combined axial force and moment. In addition, the vertical web member near the Vierendeel panel was predominantly subjected to moment, since the flexural stresses at the end sections caused by moment were larger than the stresses at the middle section caused by axial force.

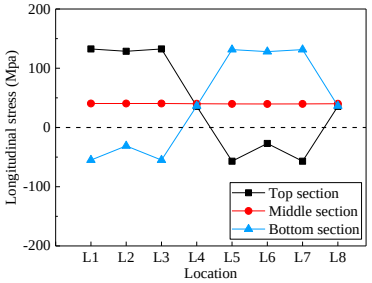

Fig. 22 Longitudinal stresses at the vertical web member

Fig. 23 shows the distribution of the longitudinal stresses at the diagonal web member near the Vierendeel panel. All the stresses were compressive stresses, ranged from -122 MPa to -79 MPa. Therefore, the vertical web member near the Vierendeel panel was subjected to axial force.

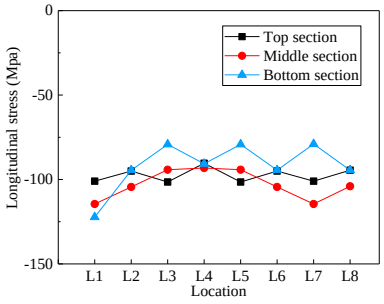

Fig. 23 Longitudinal stresses at the diagonal web member

5. Design considerations

5.1. The rigidity of the diaphragm

The classification of the in-plane rigidity of the diaphragm is required to precisely determine the lateral load on the lateral force-resisting elements and conduct an appropriate structural analysis. Diaphragms can be traditionally idealized as either “rigid”, “flexible”, or “semi-rigid” according to the relative in-plane stiffness of the diaphragms compared with the vertical elements of the lateral force-resisting system [34].

The typical RC diaphragms and concrete-filled metal decking diaphragms are idealized as rigid diaphragms provided the diaphragm span-to-depth ratio is three or less and there is no horizontal irregularity of the structure [35]. In SSTF systems, the span-to-depth ratio of the diaphragms is usually less than one, because the span of the truss is larger than the column spacing. The RC diaphragms, concrete-filled metal decking diaphragms or steel bar truss metal decking diaphragms are recommended by JGJ/T 329-2015 [30]. Therefore, in these circumstances, the diaphragms in SSTF systems are rigid.

However, the diaphragms in SSTF systems need to transfer the shear loads of the trusses due to the staggered arrangement of the trusses. In the bottom story, the diaphragms are subjected to large in-plane shear load, almost equal to the base shear of the structure. The in-plane deformation of the diaphragms need to be assessed. In addition, the diaphragm near the Vierendeel panel occurred out-of-plane damages at the plastic stage when the sub-structure subjected to lateral loads, which thereby performs like diaphragm with opening, as shown in Fig. 17.

A more explicit classification of diaphragms, as currently prescribed and as shown in Fig. 24, is based on the ratio between maximum diaphragm displacement relative to the lateral force-resisting systems (Δ_{dia}) and the corresponding average inter-story drift of the lateral force-resisting systems (Δ_{LFRS}) [35]. For rigid diaphragm behaviour this ratio (η) is expected to be less than 0.5, for flexible diaphragm behaviour greater than 2.0 and for all values in-between, the diaphragm is classified as semi-rigid [36].

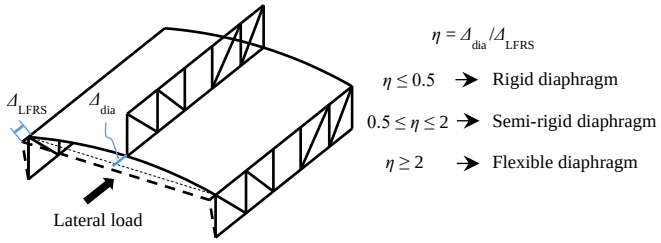

Fig. 24 Prescribed diaphragm classification

Fig. 25 depicts the transverse in-plane deformations of the diaphragms in the SSTF sub-structure model and the ratio to story drift. Though the in-plane diaphragm deformation gradually increased at the loading process, the in-plane diaphragm deformation was far less than the story drift. The ratios (η) were less than 0.13. Therefore, the RC diaphragms in SSTF systems indeed performed as a rigid plate accounting for the minor in-plane deformations. The allocation of lateral loads to each individual truss is based on the relative stiffnesses of the trusses and this principle is adopted in the Design Guide 14: Staggered Truss System Framing Systems [8] and JGJ/T 329-2015 [30]. However, it should be noted that the rigid diaphragm assumption (the out-of-plane stiffness is neglected) is not recommended for the structural analysis and design of SSTF structures. The out-of-plane stiffness of the diaphragms significantly increased the lateral stiffness of the truss and the internal forces of the web members, as discussed above. Most importantly, the use of the rigid diaphragm assumption may result in erroneous predictions of yielding mechanisms and overly underestimated predictions of base shear forces [13].

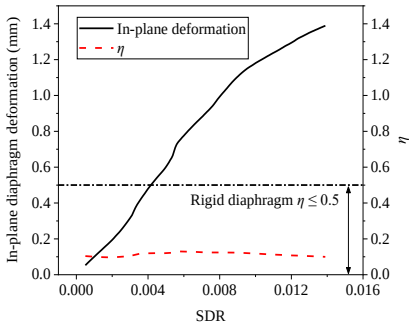

Fig. 25 In-plane deformation of the diaphragm and ratio to the story drift

5.2. The rotation demand of the chord member

As described above, the chord members of the SSTF systems are convinced of high rotation demand in order to achieve the expected ductile failure mode. As shown in Fig. 26, when the expected failure mode is achieved, the rotation of the chord member (α) is proportional to SDR (θ) [10,33].

$$\alpha = (L/s)\theta \tag{9}$$

where L and s are the truss span and the Vierendeel panel length, respectively.

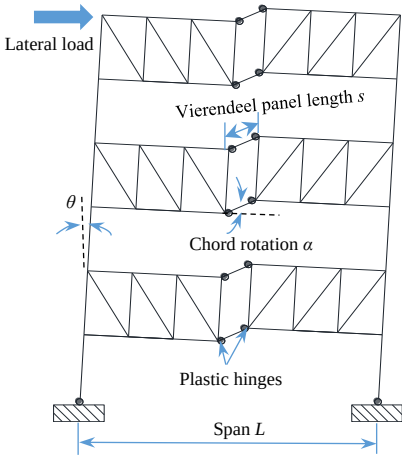

Fig. 26 Deformation configuration of a SSTF

The rotation of the chord member (α) in Eq. (9) is overvalued due to the idealized plastic hinge assumption: the flexural stiffness and length of the plastic hinge at the chord member are zero. Actually, both the steel chord member and the composite chord member with diaphragm hard to form the idealized plastic hinge. As shown in Fig. 27, the ratio of the chord member rotation to SDR of both the pure truss model and the sub-structure model were far less than the idealized ratio (L/s). For the pure truss model, the ratio was a constant value in the elastic stage. After the chord member yielded, the ratio increased with the development of the plasticity of the chord member. The ratio of the chord member rotation to SDR of the pure truss model at the plastic SDR limit was 16% lower than the idealized value. In addition, the ratio of the chord member rotation to SDR of the sub-structure model at the plastic SDR limit was 51% lower than the idealized value, because of the provided flexural stiffness of the diaphragm. The closer the actual plastic hinge is to the idealized hinge, the higher ratio (α / θ) is. A reduction factor (γ) herein is proposed to calculate the rotation demand (α_D) of the designed chord member, and γ can be taken as 0.6 when RC diaphragm or concrete-filled metal decking diaphragms are used.

$$\alpha_D \le \gamma(L/s)\theta \tag{10}$$

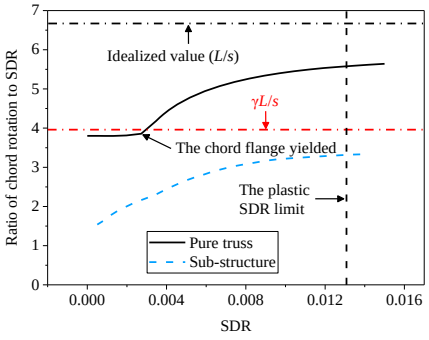

Fig. 27 The rotation of the chord member at loading process

The precise determination of the rotation demand of the chord member concerns the selecting of the section form and structural form of SSTF systems. In the reported studies, double channel sections were used for the chord member and long or multiple Vierendeel panels were used to improve the rotation capacity and reduce the rotation demand of the chord member [9,26,32,33]. However, double channel sections are inconvenient for construction and the adoption of long or multiple Vierendeel panels reduce the stiffness of the structure. Actually, the rotation demand of compact H section is sufficient for the chord members of SSTF structures with the single Vierendeel panels. For instance, the rotation of the H-sectional chord member of the sub-structure is 0.043 rad at the plastic SDR limit, approximately equal to the rotation capacity of compact H-sectional beams [37].

5.3. Mechanical calculation model

In existing studies, the vertical web members near the Vierendeel panel was commonly assumed as a two-force member. The schematic diagram of bending moment in a truss with a Vierendeel panel under horizontal load is illustrated in Fig. 28(a). There is no moment at the vertical web members. In addition, the axial forces in the vertical web member are small since the majority of the shear loads are borne by the diagonal web member when the truss is subjected to horizontal loads. In this case, the vertical web members might be designed in a relatively small size.

However, the gusset plate could transfer moments from the chord member due to its large in-plane flexural stiffness, producing stress concentrations at the vertical web member ends and the corners of the gusset plates. The schematic diagram of bending moment of a truss with fixed vertical web near the Vierendeel panel is shown in Fig. 28(b). It can be seen that the majority of the moment from the chord member is borne by the fixed vertical web member. Therefore, the web members near the Vierendeel panel should be treated as a fixed member subjected to combined axial force and moment. Unsafe designed results may be obtained when the ends of the vertical members are treated as hinged joints.

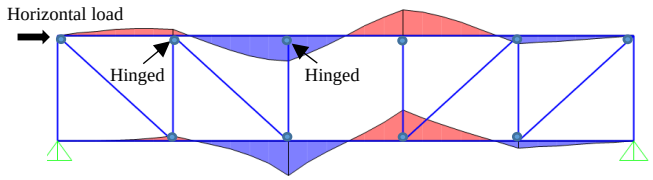

(a) with hinged vertical web near the Vierendeel panel

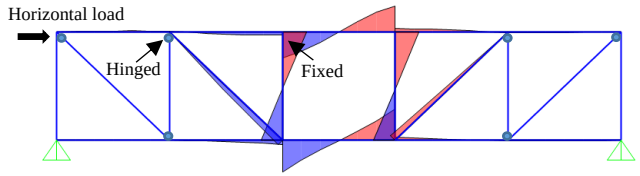

(b) with fixed vertical web near the Vierendeel panel

Fig. 28 Schematic diagram of bending moment of the truss

5.4. Amplification factor of the web members

In an SSTF system, the chord members at the Vierendeel panel are usually designed to yielded to dissipate energy and the members outside keep elastic. The maximum expected vertical shear strength of the Vierendeel panel when it is fully yielded is used to design the non-yielding members outside. The design of the web members should consider the diaphragm actions since the diaphragms significantly enhanced the strength of the Vierendeel panel by improving the flexural strength of the chord members. One practical solution is to amplify the design loads of the web members by an amplification factor when a primary design of SSTF systems was conducted. An amplification factor of 1.4 is recommended in the specification JGJ/T 329-2015 [30] to calculate the design axial load of the diagonal web member near the Vierendeel panel. However, it is an empirical value based on the findings of the premature buckling and fracture of the diagonal web members in existing tests of SSTF systems [30].

The stresses at the diagonal web member near the Vierendeel panel of the pure truss model were extracted as well, as shown in Fig. 29. The ratio of the maximum stress at the web members of the sub-structure to the pure truss was used to determine the amplification factor rather than an average value, since the web members were not permitted to yield. As seen, the ratio of the maximum stress at the diagonal web member near the Vierendeel panel of the sub-structure to the pure truss was 2.63. Therefore, a modified amplification factor of 2.7 to calculate the design axial load at the diagonal web member near the Vierendeel panel, together with the other web members, is recommended to obtain safe design results.

The flexural stresses in the web member near the Vierendeel panel of the sub-structure model shown in Fig. 30 were obtained by deducting the stresses caused by axial force (equal to the stresses at the middle section). In the same way, the flexural stresses in the web member near the Vierendeel panel of the pure truss model were obtained. The ratio of the maximum flexural stress at the vertical web member near the Vierendeel panel of the sub-structure to the pure truss was 1.57. Therefore, an amplification factor of 1.6 to calculate the design moment at the vertical web member near the Vierendeel panel is recommended.

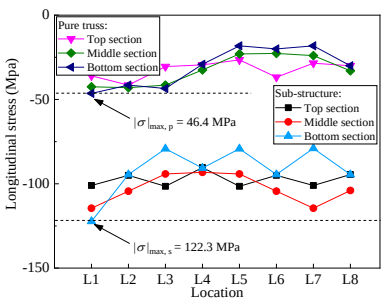

Fig. 29 Stresses at the diagonal web member near the Vierendeel panel

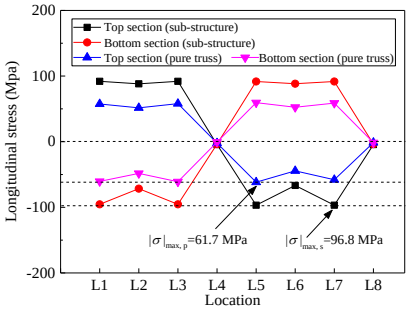

Fig. 30 Flexural stresses at the vertical web member near the Vierendeel panel

6. Conclusions

In this paper, an SSTF sub-structure for facilitating experimental research and refined FE analysis was proposed. Inelastic behavior of the proposed sub-structure was investigated by refined FE analyses. Several conclusions can be drawn.

(1) The shear force versus lateral displacement response of the truss in the sub-structure was almost the same as that in the prototype SSTF structure. The diaphragm actions in SSTF systems were well reflected by the proposed sub-structure model.

(2) The RC diaphragms increased the initial lateral stiffness and yield load of the truss by 80% and 110%, respectively. The diaphragm actions in SSTF systems should be considered when conducting structural design and analysis of SSTF systems.

(3) The RC diaphragms in SSTF systems performed as a rigid plate due to the minor in-plane deformations. The allocation of lateral loads to each individual truss of SSTF structures is based on the relative lateral stiffnesses of the trusses. The RC diaphragms can effectively transfer in-plane shear forces at the plastic SDR limit.

(4) The rotation demand of the chord member is overvalued in existing studies and H-sectional chord members is sufficient for SSTF structures with the single Vierendeel panels to realize the expected failure mode that plastic hinges only occurred in the chord members at the Vierendeel panel ends.

(5) The stresses were unevenly distributed at the vertical web members near the Vierendeel panel, exhibiting bending moment-subjecting characteristic. The web member near the Vierendeel panel should be treated as a fixed member subjected to combined axial force and moment, rather than a two-force member.

(6) A modified amplification factor of 2.7 to calculate the design axial load at the web members and an amplification factor of 1.6 to calculate the design moment at the vertical web member near the Vierendeel panel are recommended, to simply consider the diaphragm actions when conducting a primary design of SSTF systems under lateral loads.

Acknowledgements

The authors greatly appreciate the financial support provided by the National Natural Science Foundation of China (No. 52378133) and the Chongqing Natural Science Foundation of China (No. CSTB2023NSCQ-MSX0758). However, the opinions expressed in this paper are solely the authors' own

References

[1] R.J. Hansen, W.J. LeMessurier, P.J. Paul, others, New steel framing system promises major savings in high-rise apartments, Architecture Record. 139 (1966) 191–196.
[2] X. Zhou, Z. Zhou, Q. Zhou, W. Huang, W. Guo, Hysteretic behavior and design considerations of staggered truss framing systems, Journal of Building Engineering. 72 (2023) 106696. https://doi.org/10.1016/j.jobe.2023.106696.
[3] R.P. Gupta, S.C. Goel, Dynamic analysis of staggered truss framing system, Journal of the Structural Division. 98 (1972) 1475–1492.
[4] A. Brazil, Staggered truss system proves economical for hotels, Modern Steel Construction. 40 (2000) 32–39.
[5] B. Pollak, Staggered truss solution, Modern Steel Construction. 43 (2003) 38–43.
[6] R.D. Hanson, G.V. Berg, Aseismic Design of Staggered Truss Buildings, Journal of the Structural Division. 100 (1974) 175–193. https://doi.org/10.1061/JSDEAG.0003690.
[7] J. Kim, J.-H. Lee, Y.-M. Kim, Inelastic behavior of staggered truss systems, The Structural Design of Tall and Special Buildings. 16 (2007) 85–105.
[8] AISC (American Institute of Steel Construction), Steel design guide series 14: staggered truss framing systems, AISC, Chicago, IL, 2002.
[9] S. Simasathien, S. Chao, K. Moore, T. Okazaki, Modified structural layouts for staggered truss framing systems used in seismically active areas, in: Proceedings of the 10th National Conference in Earthquake Engineering, Earthquake Engineering Research Institute Anchorage, AK, 2014.
[10] J. Kim, J. Lee, B. Kim, Seismic retrofit schemes for staggered truss structures, Eng. Struct.

102 (2015) 93–107. https://doi.org/10.1016/j.engstruct.2015.08.006.
[11] J. Kim, S. Kim, Performance-based seismic design of staggered truss frames with friction dampers, Thin-Walled Struct. 111 (2017) 197–209. https://doi.org/10.1016/j.tws.2016.12.001.
[12] X. Zhou, Y. Chen, K. Ke, M.C.H. Yam, H. Li, Hybrid steel staggered truss frame (SSTF): A probabilistic spectral energy modification coefficient surface model for damage-control evaluation and performance insights, Journal of Building Engineering. 45 (2022) 103556. https://doi.org/10.1016/j.jobe.2021.103556.
[13] Z. Li, D. Gan, X. Zhou, Effects of Modeling Methods of RC Diaphragm on the Behavior of Steel Staggered Truss Framing Structures, in: G. Geng, X. Qian, L.H. Poh, S.D. Pang (Eds.), Proceedings of The 17th East Asian-Pacific Conference on Structural Engineering and Construction, 2022, Springer Nature Singapore, Singapore, 2023: pp. 1369–1381.
[14] Seismology Committee of Structural Engineers Association of California, Seismic design of staggered truss systems, Structure Magazine. (2008) 46–47.
[15] X. Zhou, Y. He, L. Xu, Q. Zhou, Experimental study and numerical analyses on seismic behaviors of staggered-truss system under low cyclic loading, Thin-Walled Struct. 47 (2009) 1343–1353. https://doi.org/10.1016/j.tws.2009.03.007.
[16] C. Chen, W. Zhang, Comparative experimental investigation on steel staggered-truss constructed with different joints in fire, Journal of Constructional Steel Research. 77 (2012) 43–53. https://doi.org/10.1016/j.jcsr.2012.05.002.
[17] C. Chen, W. Zhang, Experimental study of the mechanical behavior of steel staggered truss system under pool fire conditions, Thin-Walled Structures. 49 (2011) 1442–1451. https://doi.org/10.1016/j.tws.2011.07.004.
[18] X. Zhou, W. Huang, Q. Zhou, Z. Zhou, W. Guo, Pseudo-dynamic test and numerical analyses of staggered truss framing systems, Structures. 45 (2022) 509–522. https://doi.org/10.1016/j.istruc.2022.09.018.
[19] D.S. Simulia, ABAQUS 6.13 User's manual, Dassault Systems, Providence, RI. 305 (2013) 306.
[20] X. Qiang, F.S.K. Bijlaard, H. Kolstein, X. Jiang, Behaviour of beam-to-column high strength steel endplate connections under fire conditions – Part 2: Numerical study, Engineering Structures. 64 (2014) 39–51. https://doi.org/10.1016/j.engstruct.2014.01.034.
[21] H. Yin, G. Shi, Finite element analysis on the seismic behavior of fully prefabricated steel frames, Engineering Structures. 173 (2018) 28–51. https://doi.org/10.1016/j.engstruct.2018.06.096.
[22] ACI (American Concrete Institute), Building code requirements for structural concrete (ACI 318–19), ACI, Farmington Hills, 2019.
[23] MOHURD (Ministry of housing and urban rural development of the people's Republic of China), Code for design of concrete structures: GB50010-2010, China Construction Industry Press, Beijing, 2015.
[24] Fib Bulletins : Model Code 2010 - Final draft, Volume 1, (n.d.). https://fib-international.org/publications/fib-bulletins/model-code-2010-final-draft,-volume-1-detail.html (accessed March 23, 2023).
[25] W. Demin, H. Fukang, Investigation for plastic damage constitutive models of the concrete material, Procedia Engineering. 210 (2017) 71–78. https://doi.org/10.1016/j.proeng.2017.11.050.
[26] S.-H. Chao, C. Jiansinlapadamrong, S. Simasathien, T. Okazaki, Full-Scale Testing and Design of Special Truss Moment Frames for High-Seismic Areas, J. Struct. Eng. 146 (2020) 04019229. https://doi.org/10.1061/(ASCE)ST.1943-541X.0002541.
[27] A. Ciutina, D. Dubina, G. Danku, Influence of steel-concrete interaction in dissipative zones of frames: I–Experimental study, Steel and Composite Structures, An International Journal. 15 (2013) 299–322.
[28] Z. Tan, W. Zhong, B. Meng, Y. Zheng, S. Duan, Z. Qu, Numerical evaluation on collapse-resistant performance of steel-braced concentric frames, Journal of Constructional Steel Research. 193 (2022) 107268. https://doi.org/10.1016/j.jcsr.2022.107268.
[29] Afifi Mohamed, Tremblay Robert, Rogers Colin A., Design and Detailing Recommendations of Slotted-Hidden-Gap Connection for Square HSS Brace Members, Journal of Structural Engineering. 149 (2023) 04022249. https://doi.org/10.1061/JSENDH.STENG-11609.
[30] MOHURD (Ministry of housing and urban rural development of the people's Republic of China), Specification for design of staggered steel truss framing systems: JGJ/T 329-2015, China Construction Industry Press, Beijing, 2015.
[31] MOHURD (Ministry of housing and urban rural development of the people's Republic of China), Code for seismic design of buildings: GB50011-2010, China Construction Industry Press, Beijing, 2016.
[32] S. Simasathien, C. Jiansinlapadamrong, S.-H. Chao, Seismic behavior of special truss moment frame with double hollow structural sections as chord members, Eng. Struct. 131 (2017) 14–27. https://doi.org/10.1016/j.engstruct.2016.10.001.
[33] X. Zhou, D. Gan, J. Xi, Z. Li, K. Ke, Z. Yang, Seismic behavior analysis and energy-based design of SSTFs with multiple Vierendeel panels, Journal of Constructional Steel Research. 212 (2024) 108243. https://doi.org/10.1016/j.jcsr.2023.108243.
[34] J.P. Moehle, J.D. Hooper, D.J. Kelly, T.R. Meyer, Seismic design of cast-in-place concrete diaphragms, chords, and collectors, NIST GCR. (2010) 10–917.
[35] ASCE (American Society of Civil), Minimum Design Loads for Buildings and Other Structures: ASCE/SEI 7-16, ASCE, Reston, VA, 2016.
[36] S. Srisangeerthanan, M.J. Hashemi, P. Rajeev, E. Gad, S. Fernando, Numerical study on the effects of diaphragm stiffness and strength on the seismic response of multi-story modular buildings, Engineering Structures. 163 (2018) 25–37. https://doi.org/10.1016/j.engstruct.2018.02.048.
[37] A. Mohabeddine, Y.W. Koudri, J.A.F.O. Correia, J.M. Castro, Rotation capacity of steel members for the seismic assessment of steel buildings, Engineering Structures. 244 (2021) 112760. https://doi.org/10.1016/j.engstruct.2021.112760.